# Limited Tissue Penetration of Taxanes: A Mechanism for Resistance in Solid Tumors

Alastair H. Kyle, Lynsey A. Huxham, Devon M. Yeoman, and Andrew I. Minchinton

**Abstract**

**Purpose:** Limited drug penetration in solid tumors is a potential mechanism of resistance for many anticancer drugs. Taxanes represent a class of drugs that are currently undergoing a new round of development, but with little known of their ability to penetrate and distribute relative to blood vessels within solid tumors.

**Experimental Design:** We assessed the tissue penetration of paclitaxel and docetaxel in HCT-116 tumor xenografts and in multilayered cell culture (MCC), a three-dimensional cell culture model of the tumor extravascular compartment. In xenografts, taxanes were mapped relative to blood vessels to obtain drug profiles as a function of distance from vasculature. For MCC, cultures were exposed to stirred drug reservoirs and taxanes measured as a function of depth into tissue.

**Results:** Both taxanes exhibited limited penetration, with little drug reaching further than 100 μm into the tissue. Of the two, paclitaxel exhibited up to 2-fold greater penetration than docetaxel. Mapping tumor cell proliferation following treatment allowed the consequences of limited drug penetration to be assessed. In tumor xenografts where reduced drug exposure to cells far from vasculature is one of several factors influencing response to treatment, up to a 75% reduction in S-phase cells was achieved in cells nearest the vessels, but only 50% reduction was observed in the tissue 150 μm away. In MCC-based data, where the influence of reduced cell proliferation with depth into tissue was circumvented, a 5-fold (paclitaxel) and 10-fold (docetaxel) increase in reservoir drug concentration was required to produce a response in cells 150 μm into the tissue equivalent to that seen in cells directly exposed to the drug.

**Conclusion:** These results indicate that limited distribution is an important mechanism of tumor resistance to taxanes.

Little is known about the penetration and distribution in solid tumors of many commonly used anticancer drugs (1, 2). Although the measurement of average drug accumulation in tumors is a routine component in the development of any new anticancer drug, it may reveal very little about the ability of a drug to distribute within a tumor. This is because unlike normal tissues, the extravascular compartment of solid tumors can pose a significant barrier to drug penetration (1, 3, 4). Tumor cells can be located 15 to 20 cell diameters from the nearest blood vessel, whereas in normal tissue, cells are usually within a few cell diameters of a vessel. The tissue penetration of paclitaxel has been studied previously via the detection of radiolabeled drug in whole tumor sections (5), but without vasculature information, and also in tumor histocultures (6). These studies suggested poor penetration of paclitaxel, with buildup occurring over a period of days, although no analysis was done. Paclitaxel has been studied quantitatively, via high-performance liquid chromatography detection, in bladder tissue that was sequentially sectioned in relation to the urothelium (7, 8). Paclitaxel penetration has also been studied indirectly using average cell survival in multicellular spheroids (9) and via flux through multilayered cell cultures (MCC) (1, 9, 10), although subsequent modeling to predict drug buildup in tissue was not done.

In this study, the tissue penetration of $^{3}$H-paclitaxel and $^{3}$H-docetaxel was mapped relative to tumor vasculature by combining a film-based dry autoradiography technique with subsequent immunohistochemical detection of tumor vasculature. Superimposition and alignment of tumor vasculature and radiolabeled drug was made possible by capturing high-resolution images of entire tumor cryosections using a robotic tiling microscope. Following automated analysis of whole tumor cryosections, drug distribution was determined as a function of distance from the nearest visible blood vessel. Although mapping radiolabeled taxane distribution relative to tumor vasculature yields information about *in vivo* taxane distribution, it has the drawback of incorporating the contribution of $^{3}$H-labeled liver metabolites, which, being smaller, could diffuse more easily. To minimize this, both taxanes were labeled in the 2-benzoyl ring rather than randomly throughout the molecule. A second drawback of the technique is that drug

**Authors' Affiliation:** Department of Medical Biophysics, British Columbia Cancer Research Centre, Vancouver, British Columbia, Canada

Received 8/4/06; revised 10/13/06; accepted 2/12/07.

**Grant support:** Canadian Institutes of Health Research. L.A. Huxham is a Michael Smith Foundation for Health Research Scholar.

The costs of publication of this article were defrayed in part by the payment of page charges. This article must therefore be hereby marked *advertisement* in accordance with 18 U.S.C. Section 1734 solely to indicate this fact.

**Requests for reprints:** Andrew I. Minchinton, British Columbia Cancer Research Centre, 675 West 10th Avenue, Vancouver, BC, Canada V5Z 1L3. Phone: 604-675-8032; Fax: 604-675-8049; E-mail: aim@bccrc.ca.



doi:10.11z58/1078-0432.CCR-06-1941

penetration will seem to be increased by contributions from vessels that just lie outside of the tissue section being analyzed, the occurrence of which will increase in likelihood with increasing distance from an observed vessel. These two factors mean that the *in vivo* based detection of drug penetration will likely represent the best case scenario and might overpredict taxane tissue penetration.

To validate the tumor-based work, we employed MCC (11, 12), a three-dimensional tissue culture model, in which a disc of tumorlike tissue is grown from single cells attached to a permeable support membrane. The model has been used previously to determine flux of drugs through tumorlike tissue (13–16). Using the MCC model avoided the contributions to apparent taxane distribution from both hidden vessels and $^3$H-labeled liver metabolites. Although conceptually similar to the tumor histoculture model, the MCC model avoids potential contributions to drug penetration from the edge of the tissue from the existing vascular network in the tumor histocultures.

In addition to comparing the tissue penetration of paclitaxel and docetaxel, a secondary goal of this study was to assess the ability of a second MCC-based assay in which a drug's effect on proliferating cells is used to determine its tissue penetration (17, 18). The assay integrates overall exposure to a drug, rather than determining drug distribution at a discrete time point. Using the distribution of drug effect in tissue as an indicator of drug penetration is generally not possible due to the changes in intrinsic sensitivity of cells that accompanies the reduction in proliferation seen with depth into the tissue (19). The disc geometry of MCCs allowed this problem to be circumvented because there exist two populations of rapidly dividing cells, one on the top and one on bottom of the disc, that are separated by the thickness of the culture itself. Drug penetration was determined by exposing cultures to drug from one side and then comparing the effect on the population of proliferating cells directly exposed to the drug versus the proliferating cells located on the far side. The effect of the taxanes on proliferation was also mapped in the tumor xenografts; however, these experiments did not differentiate between drug penetration and intrinsic changes in cell sensitivity.

We compared paclitaxel penetration with that of the analogue docetaxel and also examined the effect of paclitaxel vehicle, Cremophor EL, on tissue penetration. Both taxanes exert their antimitotic effects through binding and stabilization of microtubules leading to cell cycle arrest (20). In the human colorectal carcinoma cell line used here, HCT-116, both drugs exhibit a similar $IC_{50}$ (21). However, there are numerous differences between them which might affect their tissue penetration. Docetaxel has been reported to have a higher binding affinity to microtubules as well as faster accumulation and longer retention than paclitaxel (22, 23), which might limit its ability to distribute within the tissue. In addition, *in vivo*, both drugs are highly plasma bound, with paclitaxel 88% to 98% and docetaxel ~94% (24–26). The extent and speed at which this binding occurs and the degree of reversibility for each drug could play an important role in determining the amount of free drug available for diffusion into the tissue. Paclitaxel has the added factor of its formulation vehicle, Cremophor EL, which, through micelle formation, is thought to reduce the free drug available for diffusion and increase the duration of exposure (27, 28). The tissue distribution of the two drugs and the effect of vehicle Cremophor EL were compared in HCT-116 tumor xenografts. Then, in isolation of plasma pharmacokinetics, tissue distributions were determined using MCCs under comparable exposures.

## Materials and Methods

***Reagents.*** Stock solutions were prepared of paclitaxel (Sigma-Aldrich) in Tween 80 (Sigma-Aldrich) at 12 mg/mL and Cremophor EL (Sigma-Aldrich) at 6 mg/mL and docetaxel (Sigma-Aldrich) in Tween 80 at 40 mg/mL. For tritium-based experiments, $^3$H-paclitaxel (2-benzoyl ring-3H, ART-1195, American Radiolabeled Chemicals Inc.) in ethyl acetate and $^3$H-docetaxel (2-benzoyl ring-3H, ART-1267, American Radiolabeled Chemicals Inc.) in ethanol were centrifugally evaporated at 30°C and mixed with cold drug stock at a ratio of 60 μCi/mg cold drug immediately before diluting for injection. For paclitaxel in Cremophor EL, stock was then diluted 1:1 in saline before injection for a final concentration of 3 mg/mL. For paclitaxel in Tween 80, stock was diluted 1:1 in ethanol and then 1:1 again in saline (29) for a final concentration of 3 mg/mL. For docetaxel, stock was diluted 1:3 in 13% ethanol and then 1:25 in saline, with a final concentration of 1.38 mg/mL. 5-Bromo-2-deoxyuridine (BrdUrd) was obtained from Sigma Chemical.

***Cell culture.*** HCT-116 human colorectal carcinoma cells were purchased from American Type Culture Collection. Cells were maintained as monolayers using minimum essential media (Life Technologies/BRL) supplemented with 5% bovine growth serum (HyClone) and passaged every 3 to 4 days. Multilayered cell cultures were grown using the apparatus shown in Fig. 1A as previously described (17).

***Mice and tumors.*** Female nonobese diabetic severe combined immunodeficient mice were bred and maintained in our institutional animal facility in accordance with the Canadian Council on Animal Care guidelines. The experiments described in this paper were approved by the Animal Care Committee of the University of British Columbia. Mice were allowed free access to standard laboratory rodent food and water and were used between 8 and 11 weeks of age, weighing between 20 and 28 g. For radiolabel-based work, HCT-116 cells (50 μL of $1.6 \times 10^8$ cells/mL) were implanted s.c. into the left and right sacral regions, with two mice for a total of four tumors used for each data point. For BrdUrd-based work, only one tumor was implanted per mouse, with five mice for data point. Mice were given the drug when one or both their tumors reached 100 to 150 mm$^3$ as measured using calipers of three orthogonal diameters ($a$, $b$, and $c$) using the formula volume = $\pi/6(abc)$. The mean weight (±SD) of the excised tumors was 60 ± 24 mg. For radiolabel-based work, drugs were given i.v. For BrdUrd-based work, paclitaxel in Cremophor EL and docetaxel in

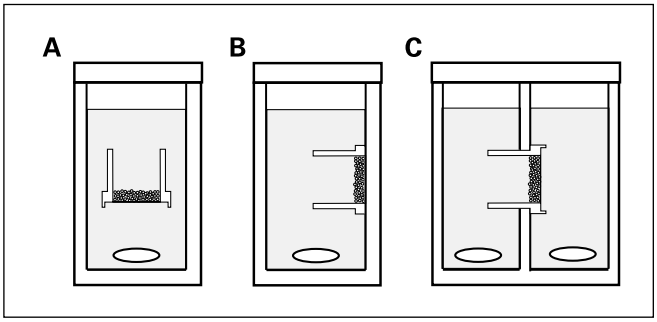


**Fig. 1.** *A,* diagram of the apparatus used during MCC growth. Up to eight MCCs are held suspended in stirred media; each has access to oxygen and nutrients from top and bottom. *B,* apparatus used to expose only one side of the cultures to drug and allow buildup in the tissue. MCC sides are defined as the near (exposed) and far (closed off). *C,* apparatus used during control experiments where cultures are exposed to drug from both sides but under differential oxygenation and glucose conditions.

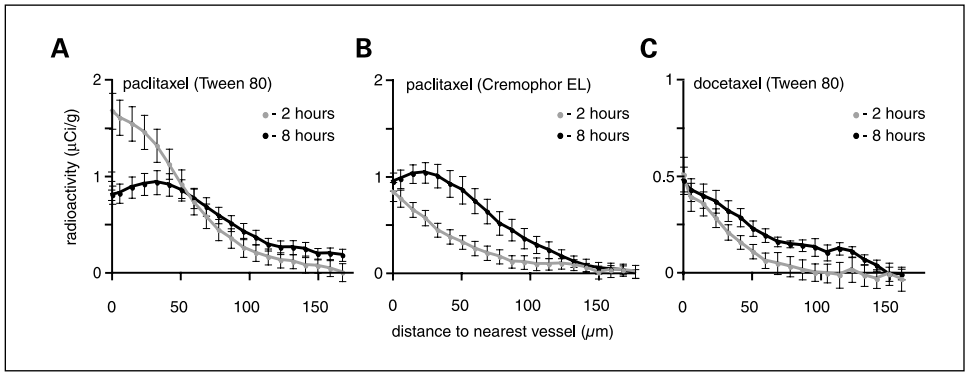


**Fig. 2.** $^3$H-taxane distribution relative to the nearest blood vessel in HCT-116 tumor xenografts 2 h (◉) and 8 h (●) following tail vein injection; 10 mg/kg paclitaxel, vehicle Tween 80 (*A*), vehicle Cremophor EL (*B*); and 5 mg/kg docetaxel, vehicle Tween 80 (*C*). Data were obtained from tritium-sensitive film clamped against 10-μm cryosections for 80 d followed by immunohistochemical staining of CD31-positive tumor vasculature. Points, average; bars, SE; $n = 9$.

Tween 80 were given i.p., and mice were given 1,500 mg/kg BrdUrd 2 h before sacrifice, as previously described (18, 30).

***MCC drug penetration assays and control assay.*** MCC drug penetration was done using the apparatus shown in Fig. 1B as previously described (17), with the following modifications. Reservoir volumes were 2.5 mL per MCC instead of the original 7.5 mL. For radiolabeled experiments, cultures were frozen immediately following the 1- or 2-h drug exposures. For the BrdUrd-based assay, following the 1-h drug exposure, MCCs were incubated for two 30-min washout periods before removal from the penetration apparatus. They were incubated for 2 days before BrdUrd labeling via exposure of both sides of MCCs to 100 μmol/L BrdUrd for 4 h and subsequent freezing. The MCC control assay was done using the apparatus shown in Fig. 1C as previously described (17). Control experiments exposed both sides of MCC to 0.1 μmol/L drug with normal conditions (20% $O_2$, 1 g/L glucose) on one side of cultures versus deprived conditions (0% $O_2$, 0.1 g/L glucose, 1 mmol/L lactate) on the other side. Three MCCs were used for each set of experimental conditions.

***Autoradiography.*** Tumor xenograft (10 μm thick) and MCCs cryosections were placed in triplicate on glass slides, allowed to dry overnight, and then clamped against tritium-sensitive film (Hyperfilm-$^3$H; GE Healthcare) under GBX filter safelight conditions (Kodak) and stored in darkness for a period of 80 days. The film was developed for 1 min using a 1:1 dilution of D-19 developer (Kodak). Calibration of film was done using a tritium standard slide with range of 0 to 489 μCi/g (American Radiolabeled Chemicals inc.).

***Immunohistochemistry.*** Cryosections were fixed in acetone-methanol for 10 min at room temperature. Vasculature was stained using an antibody to PECAM/CD31 (BD PharMingen) and fluorescent Alexa 546 anti-rat secondary antibody (Invitrogen). Slides stained for incorporated BrdUrd were placed in distilled water for 10 min and then treated with 2 mol/L HCl at room temperature for 1 h, followed by neutralization for 5 min in 0.1 mol/L sodium borate. Slides were then washed and transferred to a PBS bath. Incorporated BrdUrd was detected using a monoclonal mouse anti-BrdUrd (clone BU33, Sigma-Aldrich), followed by an anti-mouse peroxidase-conjugated antibody (Sigma-Aldrich) and a metal-enhanced 3,3′-diaminobenzidine substrate (Pierce). Slides were then counterstained with hematoxylin, dehydrated, and mounted using Permount (Fisher Scientific) before imaging.

***Image acquisition.*** The imaging system consisted of a robotic fluorescence microscope (Zeiss Imager Z1), a cooled, monochrome CCD camera (Retiga 4000R, QImaging), a motorized slide loader and *x-y* stage (Ludl Electronic Products), and customized NIH-ImageJ software[1] (public domain program developed at the NIH) running on a G5 Macintosh computer (Apple). The system allowed for tiling of adjacent microscope fields of view. Using this system, images of entire tumor cryosections up to 1 $cm^2$ and MCC sections, 0.8 cm in length, were captured at a resolution of 0.75 μm per pixel.

***Image analysis.*** Using the NIH-Image software application and user-supplied algorithms, digital images of $^3$H-taxane distributions were analyzed in the following manner. For tumors, digital images of tritium-sensitive film and CD31 immunostained tumor cryosections were superimposed and aligned. Then, each pixel making up the film image was sorted based on its distance relative to CD31-positive vasculature. Finally, the fraction of pixels from the film that were positive was tabulated as a function of distance from vasculature. Data were scaled using results for fraction-positive pixels versus radioactivity (μCi/g) using a tritium standard slide. For MCCs, digital images of tritium-sensitive film were aligned with bright-field images of unstained tissue cryosections. Pixels making up the tissue were then sorted based on distance from each edge of the section. For BrdUrd-based work, analysis was carried out as previously described (17, 18, 30).

## Results

***$^3$H-taxane distributions in tumor xenografts.*** Figure 2 shows the tumor distributions of tritium-labeled paclitaxel and docetaxel as a function of distance to the nearest blood vessel. Data show that drug accumulation is limited to the first ~100 μm of tissue, with little drug reaching 100 to 150 μm away from vessels for both drugs. The vehicle Cremophor EL, which was expected to reduce plasma levels of free paclitaxel and increase its duration of exposure, reduced tissue drug levels at the 2-h time point relative to Tween 80 by more than 2-fold (Fig. 2A and B). At the 8-h time point, paclitaxel in vehicle Tween 80 is seen to have undergone substantial washout, whereas for the Cremophor EL, vehicle data paclitaxel is still accumulating in the tissue. The drug profiles at 8 h are found to be similar. Docetaxel at the 2-h time point (Fig. 2C) is seen to fall off more sharply relative to paclitaxel. In contrast to paclitaxel in Tween 80, docetaxel showed increased accumulation at 8 h.

***$^3$H-taxane distributions in MCCs.*** Figure 3 shows the distribution of tritium-labeled paclitaxel and docetaxel in MCCs following a 1- or 2-h exposure at 0.3 or 3 μmol/L. In all cases, data show moderately lower accumulation and better penetration for paclitaxel relative to docetaxel (Fig. 3A-D). Increasing the drug concentration 10-fold from 0.3 to 3 μmol/L resulted in only a ~3-fold increase in peak tissue levels, indicating at least partial saturation of sites. At the higher concentration, both drugs show improved tissue penetration, indicating that consumption of the drugs by tissue plays an important role in limiting their penetration. The longer exposure times are seen to improve tissue distributions. Peak

[1] http://rsb.info.nih.gov/ij/

radioactivity levels were observed at a depth of ~20 μm into tissue. This was likely due to averaging over gaps in the tissue on the edge of the cultures and alignment of autoradiography images, which blurred slightly on the edges. These factors would not apply to the tumor-based work, where the peaks in radioactivity ~30 μm into tissue at the 8-h paclitaxel time point is likely caused by drug washout due to falling plasma levels.

***Comparison of xenograft and MCC-based $^3$H-taxane data.*** Figure 4 shows a comparison of tissue accumulation and depth of penetration of the drugs in the two models. Peak tissue levels (Fig. 4A) seen in the tumor xenografts were ~3-fold lower for paclitaxel and ~10-fold lower for docetaxel than the 2-h, 0.3-μmol/L MCC results. In MCCs, peak levels (Fig. 4A) did not increase when going from a 1- to a 2-h exposure ($P > 0.05$ ANOVA except for the 0.3 μmol/L docetaxel); however, total tissue radioactivity (Fig. 4B) did increase moderately (significant differences, $P < 0.005$ ANOVA, for 1-h versus 2-h exposures in all cases except for 0.3 μmol/L paclitaxel). As observed from the tissue distribution profiles (Figs. 2 and 3), the depth at which the drug levels fell to half-maximum is seen to increase with concentration (Fig. 4C). The xenografts were seen to exhibit surprisingly large penetration half-depths in comparison with the MCC-based data given their low-peak tissue levels.

***Effect-based evaluation of taxane tissue penetration in MCCs.*** Figure 5A shows the effect of docetaxel on proliferating cells in MCCs 2 days after a 1-h exposure; the 150-μm bars indicate approximate thickness of the cultures at time of exposure. MCC cryosections were immunostained for incorporated BrdUrd to show S-phase cells. Untreated cultures doubled in thickness over 2 days from the time of exposure, whereas treated cultures show an increasing reduction in growth as a function of drug concentration. To determine the penetration of the drug, cells were examined on either edge of the cultures, wherein untreated cultures similar proliferating fractions are observed. At the intermediate concentration of 0.3 μmol/L, the number of S-phase cells is clearly reduced on the near/exposed side of the culture, but only at 3 μmol/L drug is the S-phase fraction on the far side of the culture reduced.

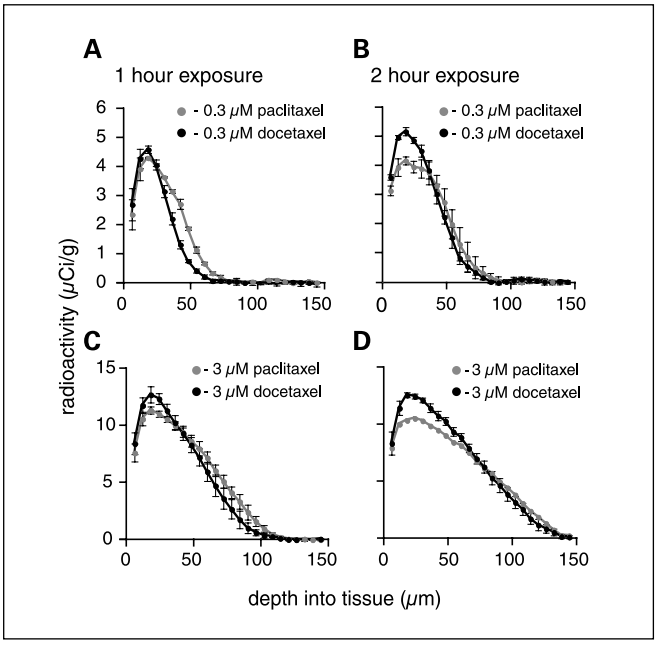


**Fig. 3.** $^3$H-taxane distribution in HCT-116 MCC following 0.3 μmol/L exposure for 1 h (*A*) and 2 h (*B*) and 3 μmol/L exposure for 1 h (*C*) and 2 h (*D*) to paclitaxel (●) and docetaxel (●). MCCs, discs of tissue grown to 150 μm, were exposed to the drug on one side, with the other side closed off to allow drug to build up. Results are shown as a function of depth into the tissue relative to the exposed side of the cultures. Points, average; bars, SE; $n = 9$.

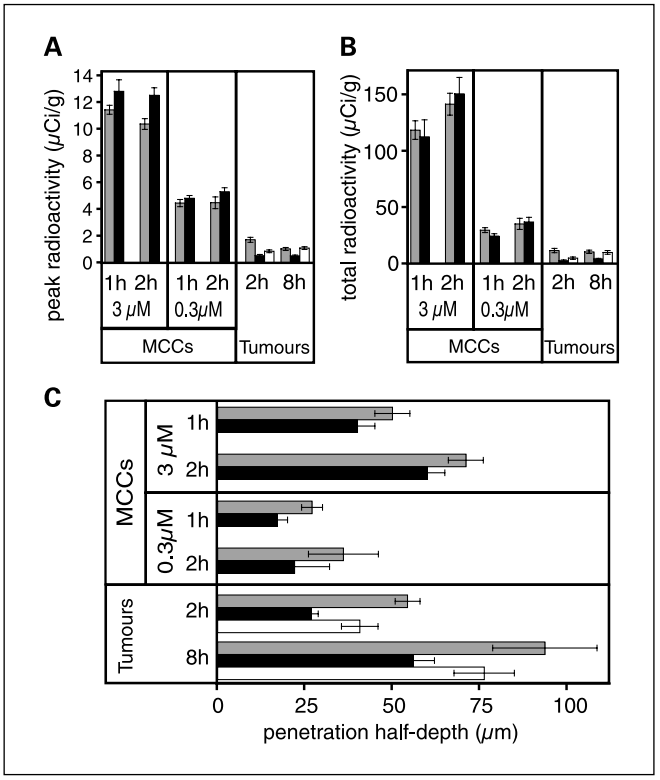


**Fig. 4.** Summary of $^3$H-taxane peak tissue levels (*A*), total radioactivity (*B*), and depth into tissue where radioactivity falls to half-maximum (*C*): paclitaxel (■), docetaxel (■), and for tumor data, paclitaxel in Cremophor EL (□).

Figure 5B and C shows results from analysis of the effect-based taxane experiments. The BrdUrd fraction in the first 30 μm of the tissue on the near/exposed versus far sides of the cultures is shown for paclitaxel (Fig. 5B, *top*) and docetaxel (Fig. 5C, *top*) as a function of drug exposure. For both drugs, a significantly greater reduction in proliferation is seen on the exposed side of the cultures. Comparison of the drug concentration required to produce a reduction in proliferation on the exposed side of the cultures as produced on the far side of cultures by the 3 μmol/L exposure indicates a ~5-fold decrease in drug exposure on the far side of the culture for paclitaxel versus ~10-fold decrease for docetaxel. Despite paclitaxel exerting a more uniform effect within the cultures, both drugs were similar in their ability to control MCC thickness (Fig. 5B and C, *bottom*). Control experiments were carried out to determine the effect that closing off the culture during drug exposure had on the response of cells on the far side. Conditions encountered on the far side of the cultures during drug exposure were simulated using the apparatus shown in Fig. 1C, in which both sides of the cultures were exposed to equal drugs, 0.1 μmol/L, but under normal conditions on the near side versus oxygen/nutrient-deprived conditions on the far side. Results, also shown in Fig. 5B and C

(*top*), indicate that temporary deprivation of oxygen and nutrients on the far side of the cultures during drug exposure did not affect the response to the drugs.

***Effect of taxanes on S-phase cell distribution in tumor xenografts.*** Before conducting the tumor-based radiolabeled drug experiments, we mapped the drug effect on S-phase cell distribution in the tumor xenografts using the same technique applied to MCCs. In these experiments, S-phase cells were mapped relative to tumor vasculature as a function of taxane dose and time following treatment, and the results are summarized in Fig. 6. Results for the time course of paclitaxel effect on S-phase cells 1, 3, and 6 days following treatment are shown in Fig. 6A, with raw data in the top and data normalized to the untreated controls in the bottom. Results show that there is a decrease in S-phase cells over the first 3 days following treatment. From the normalized data, paclitaxel is seen to produce up to a 75% reduction in proliferation near vessels, but only a 50% reduction in cells 150 μm away. Further work looking into the drug effect at the 3-day time point as a function of dose is shown in Fig. 6B for paclitaxel and Fig. 6C for docetaxel. Drug doses were chosen to span the range typically given to mice and produce equitoxic effects for the two drugs (31). From the normalized data in Fig. 6B and C (*bottom*), a preferential effect is seen on the cells in the first ~50 μm of tissue away from vessels, where proliferation and drug exposures are highest.

## Discussion

Data from both radiolabeled drug imaging and drug effect on cell proliferation showed poor distribution of the taxanes, with most drug limited to the first 100 μm of tissue. Paclitaxel penetrated further into the tissue than docetaxel, consistent with previous reports of increased cellular consumption of docetaxel (22). The greatest difference between the two drugs was seen in the effect-based assay, where paclitaxel showed a 2-fold increase in penetration relative to docetaxel. MCC-based results for both drugs showed a partial saturation of tissue binding and improved penetration at higher concentrations.

The formulation vehicle Cremophor EL had the expected effect of reducing initial peak levels of paclitaxel in tumors, but increasing its duration of exposure. It was interesting that at the 8-h time point, both paclitaxel formulations produced similar drug profiles; however, the tissue area under the curve for 0 to 8 h would still be higher for the Tween 80 data. Later time points might eventually result in greater accumulation for the Cremophor EL data.

The MCC-based work was intended to serve as a comparison between the drugs in isolation of their *in vivo* pharmacokinetic differences rather than to reproduce blood pharmacokinetic profiles. Hence, drug exposures were chosen to bracket the expected tumor exposures. However, peak tumor levels for paclitaxel and docetaxel were, respectively, ~3- and 10-fold lower than those seen in MCC following the 0.3 μmol/L exposure. This is despite reported plasma areas under the curve and peak levels in mice in the range of 35 and 5 μmol/L × h and peak levels of 40 and 10 μmol/L for paclitaxel and docetaxel, respectively (25, 29). These results indicate that blood binding of the drugs plays a significant role in limiting their tissue distribution, and that only the free form of the drug in plasma is likely to contribute to tissue penetration. MCC work was carried out in 5% serum, which likely results in ~50% unbound drug (24) as compared with 2% to 10% unbound drug expected *in vivo* (25, 26). Based on these findings, future work could be carried out to look at taxane penetration in MCCs at lower drug concentrations, matching the levels detected from the tumor-based work. Under these conditions, the taxanes might exhibit an even greater reduction in penetration or perhaps behave in a similar way to the 0.3 μmol/L data. It would also be interesting to use the assay to

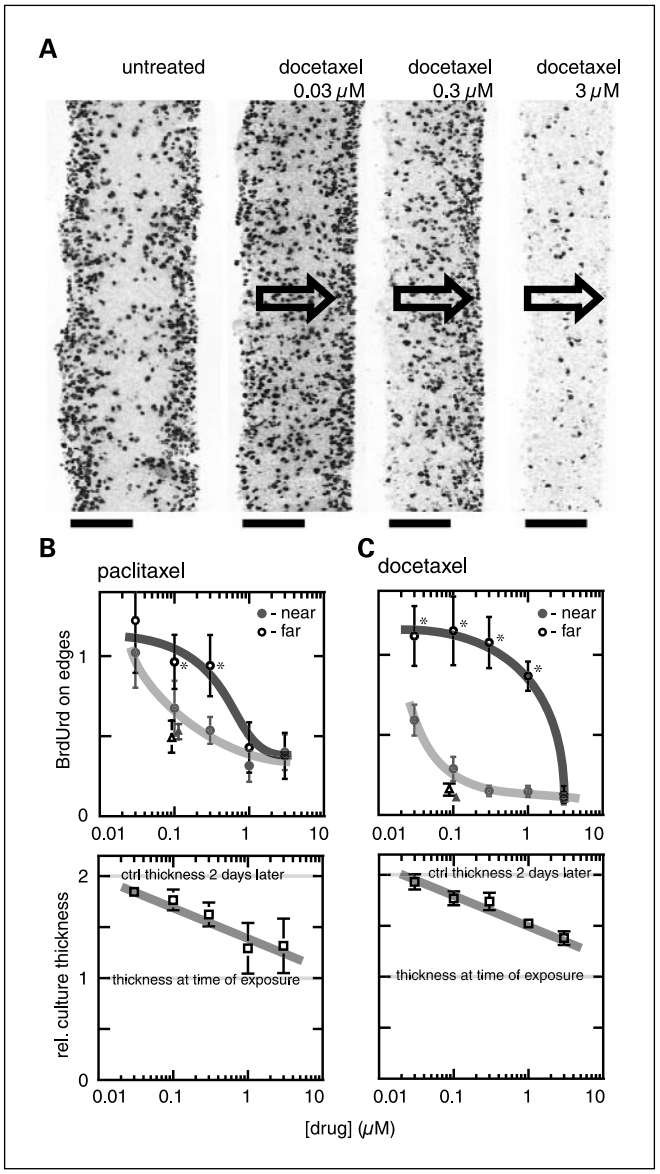


**Fig. 5.** S-phase cells in MCC 2 d after a 1-h drug exposure to one side. BrdUrd-immunostained cryosections after 0 to 3 μmol/L docetaxel (*A*). Arrows, direction of drug exposure. Bar, 150 μm, approximate thickness of cultures at time of drug exposure. Analysis of drug effect on the rapidly proliferating cells of the first 30 μm of the tissue on the near (●) and far (○) side of MCCs for paclitaxel (*B*) and docetaxel (*C*). Data show BrdUrd immunostaining expressed as the fraction of levels seen in untreated MCCs. Results from control experiments under conditions of normal (▲) versus low oxygen and glucose and high lactate (△) are also shown. Bottom, MCC thickness 2 d after treatment plotted relative to thickness at time of treatment. Points, average; bars, SE; $n = 4$-6. *, $P < 0.005$ (ANOVA), data points where the drug effect on the far side was significantly less than on the near side. The effect of paclitaxel versus docetaxel on thickness were comparable for all concentrations, $P > 0.05$ (ANOVA).

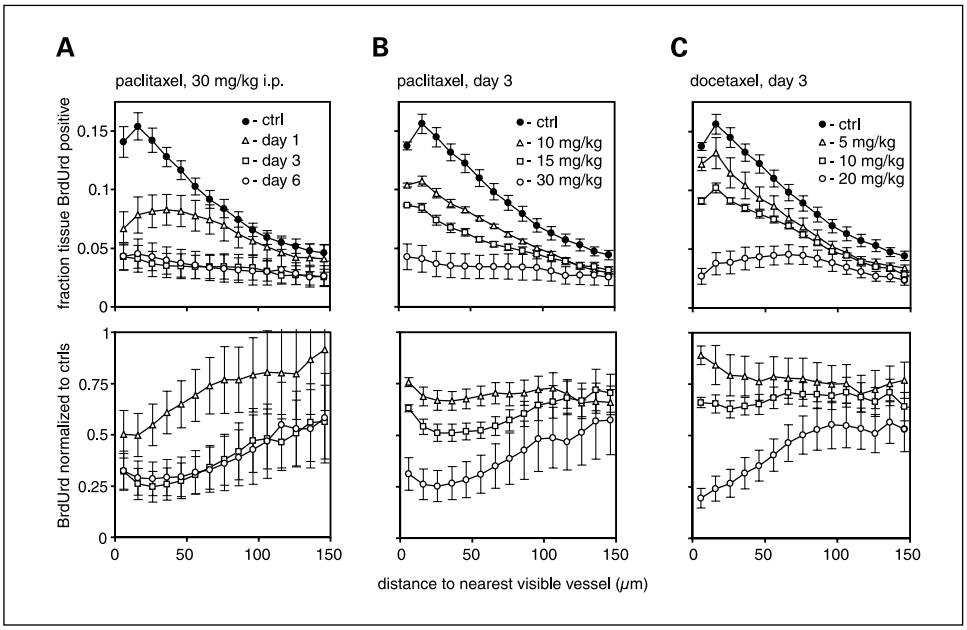


**Fig. 6.** S-phase cells seen in HCT-116 tumor xenografts following i.p. administration of paclitaxel and docetaxel. Time course for action of 30 mg/kg paclitaxel 1, 3, and 6 d following treatment (*A*) and dose response 3 d following treatment for paclitaxel, 10, 15, and 30 mg/kg (*B*), and docetaxel, 5, 10, and 20 mg/kg (*C*). Results are shown for raw data (*top*) and data normalized to controls (*bottom*), where a value of 1 indicates no change relative the untreated controls. Points, average; bars, SE; $n = 3$-5.

examine the relation between exposure duration and drug concentration on overall drug buildup at lower drug concentrations and longer exposures.

The apparent depth of penetration of the drugs in tumors as compared with MCCs was greater than expected given the marked concentration dependence of tissue penetration seen here. The radial geometry seen in the HCT-116 tumor type, in which cords of tumor cells surround individual vessels (30), should pose a greater barrier to penetration than does the planar geometry of MCC discs. Two factors might explain the increased penetration seen in the tumor data. First, there will exist unobserved vessels that lie just above or below the 10-μm tissue sections cut from the tumors. The likelihood of occurrence of unobserved vessels will increase with distance from observed ones, and hence, they will increase the apparent penetration half-depth of a drug. Another factor that might increase the apparent penetration of the taxanes *in vivo* is the contribution of $^{3}$H-labeled liver metabolites, which might diffuse more easily than the parent drug.

A unique property of the disc geometry of MCCs is that it presents a barrier to penetration in which there exist rapidly proliferating cells at two positions in the tissue (either edge). This symmetry makes it possible to use the effect of the drugs as an indicator of their penetration, in effect, using the cells themselves as the drug measurement end point. Results from the effect-based assay were interesting in that the differential in drug effect on the two edges was not as great as might be expected from the steep drug gradients observed in the autoradiography-based data. However, the radiolabeled data produced discrete snapshots of drug distribution at two time points during drug buildup, whereas the effect-based assay integrated exposure over the entire process of buildup and washout. Redistribution of the drugs during washout and differences in cellular retention of the drugs would affect results. It was also interesting that both taxanes controlled MCC thickness similarly despite their having different profiles of effect, with paclitaxel exerting a more uniform effect on both sides of the tissue, whereas docetaxel had a greater effect on the near side and less on the far side.

The proliferation-based tumor xenograft data showed that both drugs were less effective on the cells farthest from tumor vasculature. However, it was difficult to interpret these data on their own in terms of tissue penetration of the drugs because, unlike the MCC-based BrdUrd work, the cells farthest into the tissue exhibited only a fraction of the proliferation seen in those cells near vessels. The tissue farthest from vasculature will not only exhibit reduced sensitivity to the drugs but also a different lag time between drug exposure and progression through the cell cycle to $G_2$-M block (32). The fact that at the lowest doses, both drugs seemed to exert a uniform effect within the tumors, but at higher doses, a greater effect is observed near vessels (Fig. 6B and C, *bottom*) might be explained by indirect host toxicity, which could conceivably reduce proliferation throughout the tumor.

Based on the results of this study, the effect-based MCC assay could be used as a high-throughput method for screening new taxane analogues for tissue penetration. In the development of new taxanes with improved antitumor capabilities, tissue penetration would be one of many parameters that could be modified. However, for new analogues that exhibited *in vitro* efficacy and desirable *in vivo* pharmacokinetics and tolerance, knowledge of tissue penetration could provide additional criteria for selecting potential analogues to further develop. Because a drug that penetrates poorly will require a higher driving concentration from the blood to reach and kill the cells situated farthest from blood vessels, improving drug penetration could reduce system toxicity by reducing the blood drug levels required to achieve maximum response. Also, in addition to increasing the concentration of drug seen by the cells farthest from blood vessels, improved drug penetration might also increase the window of exposure of these cells to therapeutic levels of the drug, which could counter the effects of the lower S-phase fraction observed in this population.

## References


**1.** Tannock IF, Lee CM, Tunggal JK, Cowan DS, Egorin MJ. Limited penetration of anticancer drugs through tumor tissue: a potential cause of resistance of solid tumors to chemotherapy. Clin Cancer Res 2002;8: 878–84.

**2.** Minchinton AI, Tannock IF. Drug penetration in solid tumours. Nat Rev Cancer 2006;6:583–92.

**3.** Jain RK. Transport of molecules in the tumor interstitium: a review. Cancer Res 1987;47:3039–51.

**4.** Jain RK. Delivery of molecular and cellular medicine to solid tumors. Adv Drug Deliv Rev 1997;26:71–90.

**5.** Li C, Newman RA, Wu QP, et al. Biodistribution of paclitaxel and poly(L-glutamic acid)-paclitaxel conjugate in mice with ovarian OCa-1 tumor. Cancer Chemother Pharmacol 2000;46:416–22.

**6.** Kuh HJ, Jang SH, Wientjes MG, Weaver JR, Au JL. Determinants of paclitaxel penetration and accumulation in human solid tumor. J Pharmacol Exp Ther 1999; 290:871–80.

**7.** Knemeyer I, Wientjes MG, Au JL. Cremophor reduces paclitaxel penetration into bladder wall during intravesical treatment. Cancer Chemother Pharmacol 1999;44:241–8.

**8.** Song D, Wientjes MG, Au JL. Bladder tissue pharmacokinetics of intravesical taxol. Cancer Chemother Pharmacol 1997;40:285–92.

**9.** Nicholson KM, Bibby MC, Phillips RM. Influence of drug exposure parameters on the activity of paclitaxel in multicellular spheroids. Eur J Cancer 1997;33:1291–8.

**10.** Grantab R, Sivananthan S, Tannock IF. The penetration of anticancer drugs through tumor tissue as a function of cellular adhesion and packing density of tumor cells. Cancer Res 2006;66:1033–9.

**11.** Cowan DSM, Hicks KO, Wilson WR. Multicellular membranes as an *in vitro* model for extravascular diffusion in tumours. Br J Cancer 1996;74:S28–31.

**12.** Minchinton AI, Wendt KR, Clow KA, Fryer KH. Multilayers of cells growing on a permeable support: an *in vitro* tumour model. Acta Oncol 1997;36:13–6.

**13.** Kyle AH, Minchinton AI. Measurement of delivery and metabolism of tirapazamine to tumour tissue using the multilayered cell culture model. Cancer Chemother Pharmacol 1999;43:213–20.

**14.** Hicks KO, Ohms SJ, van Zijl PL, Denny WA, Hunter PJ, Wilson WR. An experimental and mathematical model for the extravascular transport of a DNA intercalator in tumours. Br J Cancer 1997;76:894–903.

**15.** Phillips RM, Loadman PM, Cronin BP. Evaluation of a novel *in vitro* assay for assessing drug penetration into avascular regions of tumours. Br J Cancer 1998; 77:2112–9.

**16.** Tunggal JK, Melo T, Ballinger JR, Tannock IF. The influence of expression of P-glycoprotein on the penetration of anticancer drugs through multicellular layers. Int J Cancer 2000;86:101–7.

**17.** Kyle AH, Huxham LA, Chiam AS, Sim DH, Minchinton AI. Direct assessment of drug penetration into tissue using a novel application of three-dimensional cell culture. Cancer Res 2004;64: 6304–9.

**18.** Huxham LA, Kyle AH, Baker JH, Nykilchuk LK, Minchinton AI. Microregional effects of gemcitabine in HCT-116 xenografts. Cancer Res 2004;64: 6537–41.

**19.** Olive PL, Durand RE. Drug and radiation resistance in spheroids: cell contact and kinetics. Cancer Metastasis Rev 1994;13:121–38.

**20.** Garcia P, Braguer D, Carles G, et al. Comparative effects of taxol and Taxotere on two different human carcinoma cell lines. Cancer Chemother Pharmacol 1994;34:335–43.

**21.** Bissery MC. Preclinical pharmacology of docetaxel. Eur J Cancer 1995;31ASuppl 4:S1–6.

**22.** Lavelle F, Bissery MC, Combeau C, Riou JF, Vrignaud P, Andre S. Preclinical evaluation of docetaxel (Taxotere). Semin Oncol 1995;22:3–16.

**23.** Kelland LR, Abel G. Comparative *in vitro* cytotoxicity of taxol and Taxotere against cisplatin-sensitive and -resistant human ovarian carcinoma cell lines. Cancer Chemother Pharmacol 1992;30:444–50.

**24.** Song D, Hsu LF, Au JL. Binding of taxol to plastic and glass containers and protein under *in vitro* conditions. J Pharm Sci 1996;85:29–31.

**25.** Sparreboom A, van Tellingen O, Nooijen WJ, Beijnen JH. Preclinical pharmacokinetics of paclitaxel and docetaxel. Anticancer Drugs 1998;9:1–17.

**26.** Goodman LS, Gilman A, Brunton LL, Lazo JS, Parker KL. Goodman & Gilman's The pharmacological basis of therapeutics, 11th ed. New York: McGraw-Hill; 2006. p. xxiii, 2021 p.

**27.** ten Tije AJ, Verweij J, Loos WJ, Sparreboom A. Pharmacological effects of formulation vehicles: implications for cancer chemotherapy. Clin Pharmacokinet 2003;42:665–85.

**28.** Gelderblom H, Verweij J, van Zomeren DM, et al. Influence of Cremophor EL on the bioavailability of intraperitoneal paclitaxel. Clin Cancer Res 2002;8: 1237–41.

**29.** Sparreboom A, van Tellingen O, Nooijen WJ, Beijnen JH. Nonlinear pharmacokinetics of paclitaxel in mice results from the pharmaceutical vehicle Cremophor EL. Cancer Res 1996;56:2112–5.

**30.** Kyle AH, Huxham LA, Baker JH, Burston HE, Minchinton AI. Tumor distribution of bromodeoxyuridine-labeled cells is strongly dose dependent. Cancer Res 2003;63:5707–11.

**31.** Nicoletti MI, Lucchini V, D'Incalci M, Giavazzi R. Comparison of paclitaxel and docetaxel activity on human ovarian carcinoma xenografts. Eur J Cancer 1994;30A:691–6.

**32.** Lopes NM, Adams EG, Pitts TW, Bhuyan BK. Cell kill kinetics and cell cycle effects of taxol on human and hamster ovarian cell lines. Cancer Chemother Pharmacol 1993;32:235–42.